NANO LETTERS

2007
Vol. 7, No. 6
1749−1756

Pulsed-Interleaved Excitation FRET Measurements on Single Duplex DNA Molecules Inside C-Shaped Nanoapertures

Samantha Fore,*,† Yin Yuen,‡ Lambertus Hesselink,§ and Thomas Huser†,||

NSF Center for Biophotonics Science and Technology, University of California at Davis, 2700 Stockton Boulevard, Suite 1400, Sacramento, California 95817, Department of Applied Physics, 316 Via Pueblo Mall, Stanford University, Stanford, California 94305, Department of Electrical Engineering, Center for Integrated Systems, Stanford University, 420 Via Palou Mall/CIS-X Room 325, Stanford, California 94305, and Department of Internal Medicine, Division of Endocrinology, Clinical Nutrition, and Vascular Medicine, University of California at Davis, 4150 V Street, Suite 400, Sacramento, California 95817

Received April 6, 2007; Revised Manuscript Received April 23, 2007

ABSTRACT

Single-molecule fluorescence resonant energy transfer (FRET) is a widely accepted method for determining the spatial separation between molecules. In combination with pulsed interleaved excitation (PIE), additional information about the stoichiometry of molecular interactions is obtained. PIE-FRET, however, as implemented with standard confocal optics, requires the dilution of the sample to biologically low concentrations. Here, we show that PIE-FRET measurements inside nanometer-sized apertures yield meaningful biochemical data at 1000× higher concentrations.

Distance and interaction measurements at the molecular level are increasingly utilizing advanced optical microscopy and spectroscopy techniques, e.g., fluorescence resonance energy transfer (FRET), because only such optical techniques enable experimental studies of molecular dynamics in vitro or even in living cells.[1−3] FRET describes the radiationless transfer of excitation energy from a donor fluorophore to an acceptor fluorophore. This requires that the emission and excitation spectra of both fluorophores exhibit significant spectral overlap and that the interaction decays with $1/R^6$, where R is the distance between the fluorophores. The first experiments to determine interactions between single DNA molecules by FRET, or single-pair FRET (spFRET), were conducted by Ha et al.[4] Since then, spFRET has been widely expanded and is now applied to the investigation of macromolecular conformations and their dynamic changes as well as molecular interactions between proteins, DNA, RNA, and peptide molecules.[5−11] In the first spFRET experiments, laser excitation of just the donor molecule was employed, and the resulting fluorescence emission intensities of both donor and acceptor molecules were then used to calculate their energy transfer efficiency, E. These experiments produced accurate values for the distance between individual donor and acceptor molecules and their relative fluctuations rather than the usual average values obtained by bulk FRET measurements. This quality has turned spFRET into a useful spectroscopic ruler for interactions between individual biomolecules. Furthermore, it has also allowed for the characterization of distributions of single-pair FRET values, which enables population analyses. spFRET measurements that only excite the donor molecule, however, are still amenable to problems resulting from ambiguity in sample preparation. For example, incomplete labeling, fluorescent dye photophysics, and acceptor or donor photobleaching all lead to a population of molecular species with apparently low FRET efficiency, which is not representative of the actual interaction process. Furthermore, spFRET does not provide a general platform for the quantitative analysis of molecular interactions, i.e., the stoichiometry of interactions. These shortcomings were recently addressed with the introduction of alternating laser excitation FRET (ALEX-FRET), first developed by Kapanidis et al.[12]

* Corresponding author. E-mail: srfore@ucdavis.edu. Telephone: 916-734-8600. Fax: 916-703-5012.
† NSF Center for Biophotonics Science and Technology, University of California at Davis.
‡ Department of Applied Physics, Stanford University.
§ Department of Electrical Engineering, Stanford University.
|| Department of Internal Medicine, University of California at Davis.

10.1021/nl070822v CCC: $37.00
Published on Web 05/16/2007

Table 1. Sequence of the DNA Fragments Used for FRET Measurements inside Nanoapertures

strand	sequence (labeled nucleotides highlighted in bold, subscript denotes acceptor position)
donor	5′ CCTGAGCGTACTGCAGGATAGCCTA**T**CGCGTGTCATATGCTGTTCAGTGCG 3′
acceptor	5′ CGCACTGAACAGCATATGACACGCGA$\mathbf{T_0}$AGGCTATCC$\mathbf{T_{10}}$GCAGTACGC$\mathbf{T_{20}}$CAGG 3′

By alternately exciting both donor and acceptor molecules in a complex, it is possible to rapidly sort single molecules into two-dimensional distributions based on their donor−acceptor distance by using energy transfer efficiency (*E*) calculations and donor−acceptor stoichiometry (*S*) based on a ratiometric calculation similar to *E* as described below. The stoichiometry parameter can only be determined using the additional fluorescence component from the direct excitation of the acceptor molecule. This concept was subsequently demonstrated using the combination of time-correlated single photon counting (TCSPC) techniques and two ps-pulsed diode lasers as interleaved donor and acceptor excitation sources, a scheme known as nanosecond-ALEX[13] or pulsed interleaved excitation FRET (PIE-FRET).[14] Since then, this technique has been further refined using more sophisticated analysis methods, providing more accurate measurements of *E* and *S*.[15,16] PIE-FRET has recently been applied in a number of quantitative biological experiments (see refs 17−20). Furthermore, PIE-FRET has been extended to interactions between more than two FRET molecules, i.e., FRET interactions among three different dyes.[21,22]

Alternating laser-excitation FRET and PIE-FRET as described above still have the fundamental drawback that they require experiments to be performed at single-molecule conditions, requiring spatial separations between molecules that are larger than the physical dimensions of the laser spot. In standard confocal microscopes with diffraction-limited laser spot sizes on the order of hundreds of nanometers, this requires sample concentrations that are often well below biologically relevant equilibrium binding conditions (10^{-9}−10^{-11} M). Most protein−protein interactions, however, occur at much higher concentrations inside living cells or in whole organisms. To increase this concentration limit, the physical detection volume needs to be reduced. One technique that can achieve this involves the use of nanometer-scale apertures fabricated in thin metal films on a transparent substrate, also termed "zero-mode waveguides". This technique, which effectively extends the long-known principles of near-field optics to FCS, was first demonstrated by Levene et al.[23] It was shown that, by using approximately 50 nm diameter holes prepared in aluminum by electron beam lithography, the detection volume could be reduced to the zeptoliter range. Inside these apertures, FCS measurements could be conducted at micromolar concentrations while still observing only one molecule at a time. The small lateral dimensions of these holes thus yield effective probe volumes that are at least 3 orders of magnitude smaller than the diffraction-limited focus of a laser beam.

The fact that this method can indeed be used in practical biological applications was also demonstrated by Levene et al., who studied single-molecule polymerase activity inside their zero-mode waveguide devices by observing the incorporation of fluorescently labeled nucleotides to a growing DNA chain, a reaction that normally requires micromolar concentrations of the nucleotides. In other applications, Samiee et al. observed the diffusion of labeled membrane proteins in a lipid bilayer that had invaginated into a zero-mode waveguide,[24] and Wenger et al. observed the diffusion of lipids and GFP-tagged membrane proteins in the membranes of cells suspended across nanoaperture arrays.[25] The use of these nanoapertures for various applications has been significant enough that two reviews have already been published summarizing their usage in applications ranging from optoelectronics to biophysics.[26,27]

To access the nanomolar to micromolar equilibrium binding concentration range with single-molecule PIE-FRET techniques, we demonstrate here their combined use with nanoapertures. We show that apertures milled in a 100 nm thick aluminum film based on focused ion beam (FIB) technology enables the fabrication of apertures of arbitrary geometry or size down to ∼20 nm for biological FRET measurements. Specifically, we have investigated the application of both square and C-shaped apertures.[28] For our current application, which only makes use of visible excitation wavelengths, we show that there is no difference between the two aperture geometries. C-apertures will prove particularly important for measurements at near-infrared wavelengths because of their potentially significantly higher throughput in this range.[29] We also demonstrate that the PIE-FRET concept can be further extended to significantly higher sample concentrations (at 1000-fold) if conducted inside nanometer-sized apertures.

Materials and Methods. *DNA Samples*. Double-stranded DNA constructs have been designed with one donor fluorophore, Alexa 488, and one acceptor, Alexa 647, at varying distances, such that the dyes are either directly across from each other on the duplex DNA strand or separated by 10 or 20 base pairs (see Table 1). Donor-only and acceptor-only constructs with the same sequences were also studied. All fluorescently labeled oligos were purchased from IBA GmbH, Goettingen, Germany. The strands were annealed at 1 μM concentration using a 50% molar excess of donor strand, in 40 mM Tris, 1 mM EDTA, 500 mM NaCl buffer, and by heating to 90 °C for 5 min followed by slow cooling to room temperature. Samples prepared in this manner were then stored at 4 °C until their use in single-molecule experiments. DNA duplex strands were diluted in a Hepes-NaOH buffer (10 mM Hepes-NaOH, pH 7.4/500 mM NaCl/100 μg/mL BSA) to achieve a final concentration of 50 pM and 250 nM for either the diffraction-limited volume or the nanoaperture measurements, respectively. For consistency, we will label the different FRET duplex samples by "DA" followed by a subscript number that indicates the number of base pairs separating the dye-labeled bases. The high FRET sample will thus be labeled DA_0, the medium FRET

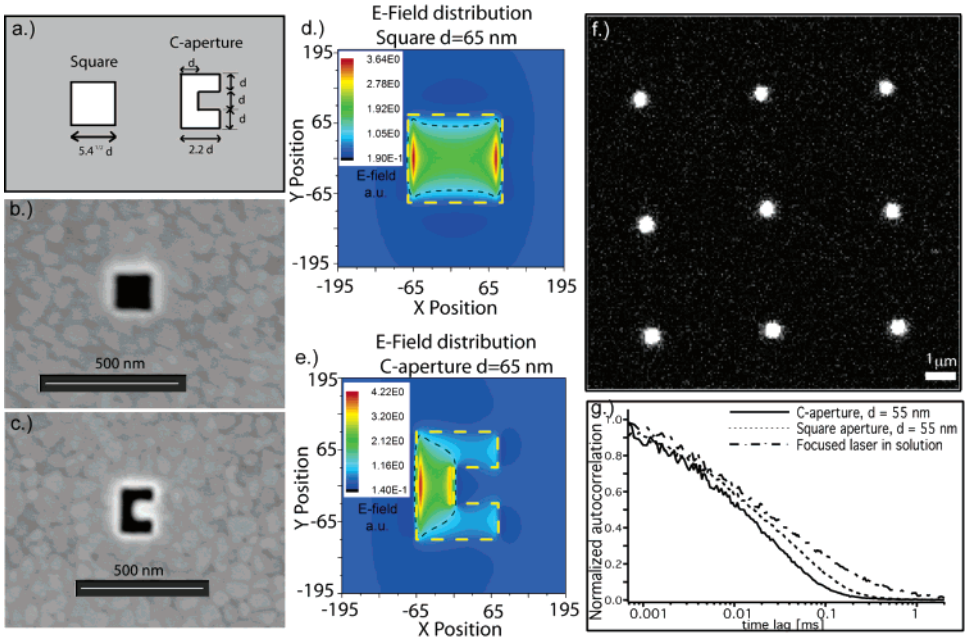

Figure 1. (a) Schematics of the nanoaperture samples. Apertures of different shape (square or C-shaped) and different dimensions (axis length d) are milled into an aluminum film on a fused silica substrate. (b) High-resolution SEM micrograph of a square aperture. (c) High-resolution SEM micrograph of a C-shaped aperture. (d,e) FDTD simulations for the Ex component of the E-field distribution inside the nanoapertures for (d) a square aperture with $d = 65$ nm (156 nm × 156 nm) and for (e) a C-aperture with $d = 65$ nm. The yellow dashed outlines are graphic overlays of the aperture geometry, and the black dashed lines are constant electric field contours which enclose regions of space with field amplitude above 1. (f) Optical scan of a section of the sample containing square apertures. The apertures are filled with a fluorescent dye to highlight their location. (g) Fluorescence correlation spectroscopy (FCS) curves comparing Alexa 488 dye diffusion inside square apertures with that in C-shaped apertures. Also shown is an FCS curve from a similar sample obtained inside a focused laser spot of dimensions ~180 nm at a concentration of 500 pM.

sample will be labeled DA_{10}, and the low FRET sample will be labeled DA_{20}.

FIB-Milled Nanoaperture Fabrication. FIB-milled apertures were fabricated as described in detail in ref 28. Briefly, a quartz glass or fused silica substrate is cleaned in a piranha solution of H_2SO_4:H_2O_2 of 4:1 concentration for 20 min to strip it of any organic contaminants. Subsequently, the sample is rinsed twice in running DI water for 5 min each and then air-dried. The cleaned sample is mounted onto silicon carrier wafers for RF sputter-coating with aluminum. For our experiments, the Al film thickness is set to 100 nm. Apertures are milled in the Al layer using an FEI Strata 235DB FIB with 30 keV Ga^+ ions at a beam current of 10 pA. Apertures with feature sizes ranging from 50 to 100 nm were milled in increments of 5 nm. The squares have equal cross-sectional areas compared to the C apertures. The aperture geometry is shown in Figure 1a, and SEM images of a square and C aperture are shown in Figure 1b and c, respectively. The dimensions are given in units of d, and this is also the value used when referring to a given aperture's size. As can be seen in Figure 1a, the square length is actually $\sqrt{5.4}d$. Finite-difference time-domain (FDTD) simulations are shown in Figure 1d and e for the E_x component of the E-field distribution inside the nanoapertures for a square aperture with $d = 65$ nm (156 nm × 156 nm) and for a C-aperture with $d = 65$ nm, respectively, with an electric field polarized along the x-axis at 470 nm wavelength. For more details about FDTD simulations, see Supporting Information. The aperture array used in our studies is imaged with confocal scanning fluorescence microscopy and shown in Figure 1f. The fluorescence correlation spectroscopy (FCS) results for data acquired in $d = 55$ nm square and C-apertures, using free Alexa Fluor 488 (Invitrogen) dye, are shown in 1 g and will be discussed below in the Results section. PIE-FRET experiments were conducted in both square and C apertures. However, as the results were similar for both apertures, only PIE-FRET data acquired in 65 nm C-apertures will be shown in the results section.

Data Acquisition. All single-molecule experiments were conducted on a MicroTime 200 confocal fluorescence microscope system (PicoQuant GmbH, Berlin, Germany) equipped with pulsed diode lasers for PIE-FRET and time-correlated single-photon counting electronics for time-resolved measurements. The donor dye was excited with a 470 nm pulsed diode laser (~80 ps pulse length) at 100 μW average excitation power. The acceptor dye was excited with a 640 nm pulsed diode laser at 60 μW average excitation power. The lasers were each triggered with a repetition rate of 20 MHz, and the 470 nm laser pulse was delayed by 25 ns with respect to the 635 nm laser, to produce a total excitation repetition rate of 40 MHz for both lasers taken together. For the standard PIE-FRET experiments in a diffraction-limited volume, the laser was focused through an Olympus 1.45 NA 100× oil immersion objective to a tight spot at a height of approximately 5 μm above a glass coverslip surface. Using FCS measurements of Rhodamine 6G molecules in water, the effective volume V_{eff} at 470 nm excitation wavelength was determined to be 0.2 femtoliter.

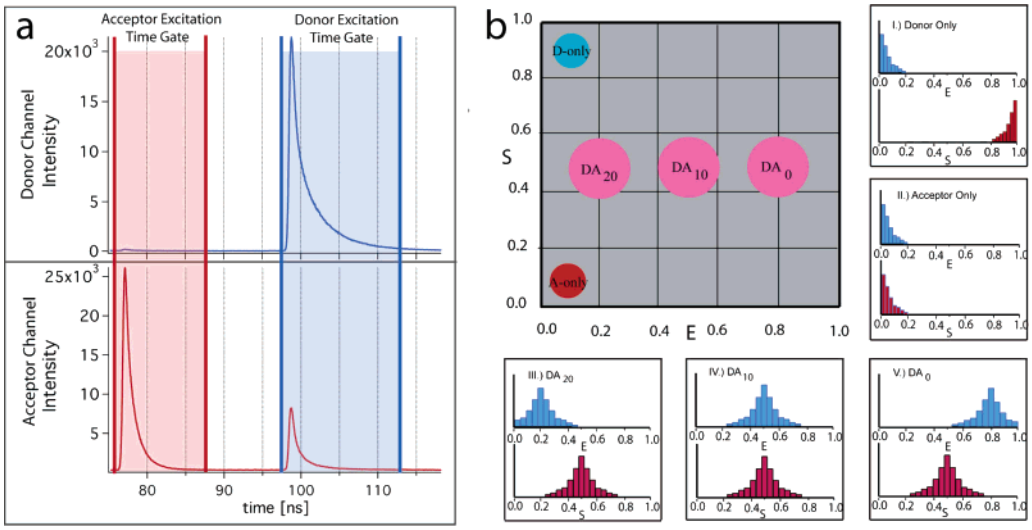

Figure 2. (a) Schematics of pulsed-interleaved excitation (PIE) FRET with time-correlated single photon counting (TCSPC). Pulses from two picosecond diode lasers with different excitation wavelengths (red: 640 nm; blue: 470 nm) are interleaved and detected at different "start" times by the TCSPC electronics. Direct acceptor dye excitation leads to the detection of fluorescence photons in just the acceptor channel, whereas excitation of the donor dye can lead to fluorescence detection in both (acceptor and donor) channels. Photons obtained by either acceptor or donor excitation can be separated by time-gating based on their photon arrival time. (b) Example of an $E-S$ histogram based on the different fluorophore-labeled DNA samples of relevance for this paper. FRET efficiency (E) and stoichiometry (S) for many single-molecule events are combined into a 2-D scatter plot. Depending on the sample donor−acceptor distance, different scenarios are shown as example 1-D E and S histograms and their respective locations in the 2-D histogram.

For the experiments with the FIB-milled apertures, the laser was focused at the interface between the fused silica surface and the aluminum film. In all cases, the donor and acceptor fluorescence emission was split by a dichroic beam splitter (600DCXR, Chroma Tech. Corp.), spectrally filtered with emission bandpass filters (HQ520/40 m and HQ680/75 m, Chroma Tech. Corp., for the donor and acceptor emission, respectively), and detected by single-photon counting avalanche photodiodes (SPCM-AQR-14, Perkin-Elmer). The signals from the detectors are sent into a four-way router and processed by a time-correlated single-photon counting board (TimeHarp200, PicoQuant), operating in time-tagged time-resolved (TTTR) mode. The TTTR mode of the data acquisition records the timing information for each photon, i.e., a macro-time stamp at 100 ns resolution and a start−stop event time referenced by the laser pulse, and the detection channel which received the photon count with 32 ps time resolution. This method of data collection enables flexible analysis modes of the full data set, which are needed to perform PIE-FRET measurements and the construction of 2-D PIE $E-S$ histograms. FCS can be simultaneously conducted using this mode of data collection, and autocorrelation curves, $G(\tau)$, generated from the data analysis be used to determine particle number, N, and diffusion times, τ_D. The TTTR data are collected for a total of 10 min for the experiments conducted inside a diffraction limited volume and 5 min for those inside the apertures. The shorter acquisition time was used to ensure that the aperture did not drift out of the laser focus during the duration of the experiment. The principles of TCSPC-based PIE-FRET are schematically shown in Figure 2.

PIE-FRET with TCSPC. TCSPC of separate detection channels allows for the temporal analysis of all detected photons. In particular, it enables the determination of which excitation laser (470 or 640 nm) leads to the detection of a photon. In practice, this is achieved by binning the TCSPC (start−stop) time of all detected photons, which leads to the generation of two fluorescence lifetime decay curves corresponding to blue and red excitation in the TCSPC histogram window (see Figure 2a). Time-gating in software based on these two decay curves enables the separation of the fluorescence based upon which laser was responsible for the excitation, i.e., F_{Dex} leading to fluorescence after donor excitation and F_{Aex} leading to fluorescence after acceptor excitation. These two components can be further separated based upon the emission channel in which the fluorescence was detected, yielding in total four components: F_{Dex}^{Dem} for donor fluorescence with donor excitation, i.e., direct donor emission, F_{Dex}^{Aem} for acceptor fluorescence with donor excitation, i.e., FRET, F_{Aex}^{Aem} for acceptor fluorescence with acceptor excitation, i.e., direct acceptor emission, and F_{Aex}^{Dem} for donor fluorescence with acceptor excitation, i.e., a crosstalk term that can generally be neglected (see Figure 2a). The energy transfer efficiency and stoichiometry ratio can be calculated as described by Kapanidis et al.[12] The FRET efficiency, E, and the stoichiometry term, S, are then given by the following expressions.

$$E = \frac{F_{Dex}^{Aem}}{F_{Dex}^{Aem} + \gamma F_{Dex}^{Dem}} \tag{1}$$

$$S = \frac{F_{Dex}}{F_{Dex} + F_{Aex}} \tag{2}$$

$$\gamma = \frac{\phi_D \eta_D}{\phi_A \eta_A} \tag{3}$$

where γ is a factor that corrects for the relative detection

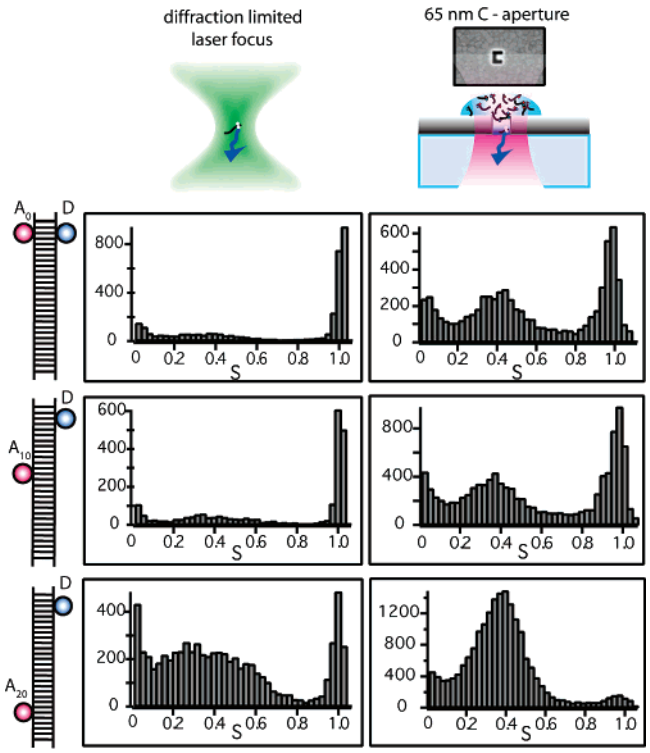

Figure 3. One-dimensional *S* histograms for donor- and acceptor-labeled DNA duplexes. The left column shows histograms of measured *S* values for experiments conducted in a diffraction-limited laser focus at 50 pM sample concentration. The different dye separations are shown schematically next to the histogram plots. The column on the right-hand side shows corresponding *S* histograms from experiments conducted inside C-shaped apertures with $d = 65$ nm at a sample concentration of 50 nM. Peaks near the center of the graphs indicate FRET events, whereas peaks near $S = 0$ or $S = 1$ are due to lone acceptor-only or donor-only events.

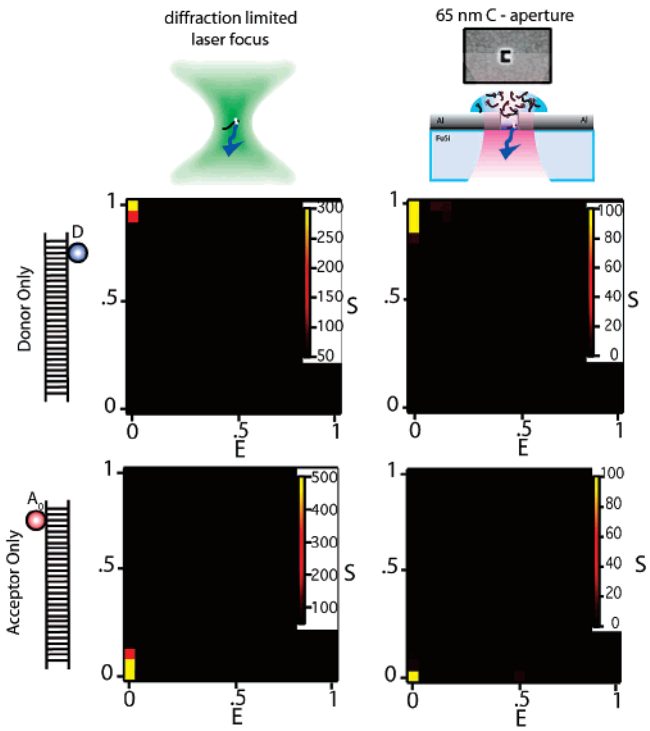

Figure 4. Two-dimensional $E-S$ histograms from PIE-FRET measurements carried out on donor-only and acceptor-only control samples as indicated by the cartoons to the left of the figure. The left column shows data obtained inside a diffraction-limited laser focus, while the right column is shows data obtained inside a C-aperture.

efficiencies, η_i, and quantum yields, ϕ_i, of the donor and acceptor dyes. In our specific case, we have assumed γ to be 1. Because the excitation and emission spectra of the dye pair that we have used are relatively well separated, crosstalk and leakage terms that are often incorporated into PIE-FRET analysis (see Lee, et al.[16] and Ruttinger, et al.[15]) can be neglected. As molecules pass through the excitation volume, discrete fluorescence bursts with a width that reflects the residence time of the molecule within the focal volume are detected. At concentrations that correspond to less than one molecule or molecular complex per focal volume, each fluorescent burst can be assigned to just a single event. Analysis of these bursts according to eqs 1 and 2 yields calculated values of *E* and *S* for each individual complex. The *E* and *S* values for each individual complex can be binned into a 2-D histogram, allowing populations of molecules to be rapidly characterized and separated based on donor−acceptor distance and donor−acceptor stoichiometry. Figure 2b shows an example of a theoretical $E-S$ histogram illustrating where populations with expected *E* and *S* values will lie on the diagram. For more information on how *E* and *S* values are calculated and how $E-S$ histograms are generated from the data set, see Supporting Information.

Results. *Fluorescence Correlation Spectroscopy of Free Dye Molecules inside Nanoapertures.* FCS measurements of free Alexa488 dye, diluted into the same Hepes buffer as used in PIE-FRET experiments, were conducted in both square and C-apertures over a range of *d*-values and then compared to FCS results in a diffraction-limited laser focus. Figure 1e shows the normalized autocorrelation curves for both square and C-apertures ($d = 55$ nm) compared to those obtained from a diffraction limited laser focus using the same dye. Measurements were conducted at 0.5 μM inside the apertures and at 500 pM inside the laser focus. Comparing the curves, we see that the diffusion time (the value of τ at which $G(\tau) = {}^1/_2$ maximum) is shorter for both square and C-apertures than for diffusion in a diffraction limited laser focus. Although both apertures have equal cross-sectional areas, the diffusion time in the C-aperture appears to be shorter. This is not altogether surprising because a quick inspection of the FDTD results in Figure 1f,g reveals that, in the C-aperture, the *E*-fields cover a region approximately half of that of a square. This translates to about a factor of 2 in the reduction of V_{eff}, as observed in the experimental FCS traces, and agrees with a lower diffusion time observed in the C-apertures when compared to the equal cross-sectional area squares.

PIE-FRET Measurements on Duplex DNA inside Nanoapertures. DNA strands were annealed with a 50% molar excess of the donor-labeled strand, using the amount in moles given on the product information sheet to calculate concentrations. A donor-only species yields an *S* ratio of approximately 1 and an acceptor-only species yields an *S* ratio of 0. For the high FRET sample, where both donor and

acceptor dyes are bound to opposite bases (DA_0) as well as for the sample where the fluorophores are separated by 10 base pairs (DA_{10}), Figure 3 shows quite clearly a large population of species with $S = 1$ due to excess free donor strands present in the sample for both the diffraction-limited laser spot (Figure 3, left column) and the C-aperture (Figure 3, right column). Surprisingly, the low FRET sample DA_{20} (acceptor and donor separated by 20 base pairs), however, appears to not have been annealed with the assumed 50% molar excess of donor strand, which we believe is either an error in the value reported in the product info sheet or an error in sample preparation. Measurements repeated in a diffracted limited laser focus with the same samples yielded the same results for *S*. A comparison of *S* values for the sample for measurements conducted in the laser spot versus the aperture indicates that, in the aperture, a greater majority of the DNA species appears to exist as donor−acceptor pairs, i.e., fully hybridized DNA duplexes, with an *S* ratio distribution center around 0.4. If we assume approximately equal conditions (buffer conditions, temperature, sample preparation) for all samples, this observation implies that, at the low concentration required for single-molecule measurements inside a laser spot, the DNA duplex appears to become unstable and undergoes partial denaturization. Hence, this is a clear demonstration of the incompatibility of biological interactions with the concentration limits imposed on single-molecule measurements conducted in standard FCS and PIE-FRET in a diffraction-limited laser spot. The same results were obtained upon repeating experiments under the same set of conditions.

Combined with the FRET efficiency *E*, such data can be plotted as two-dimensional distributions that allow one to isolate different molecular species. This is first demonstrated in Figure 4 for different donor-only and acceptor-only DNA samples. To confirm that populations with *E* values of 0 and *S* values of either 0 or 1 can be assigned to acceptor-only or donor-only species, respectively, PIE-FRET measurements were conducted on DNA duplex oligomers with the same sequence and dye positions but lacking either donor or acceptor dye. Measurements were conducted both inside a C-aperture and inside a diffraction-limited laser spot for comparison. As can be seen from Figure 4, in both cases and at both high and low concentration, all of the acceptor-only species lie in the region on the *E*−*S* histogram corresponding to $E = 0$ and $S = 0$, and all of the donor-only species lie in the region corresponding to $E = 0$ and $S = 1$, as expected for both excitation volumes.

Figure 5 shows *E*−*S* histograms for different donor−acceptor distances along the DNA duplex. The column on the left-hand side of Figure 5 displays PIE-FRET results obtained in a focused laser spot and compares them to results obtained at 1000× higher concentration in nanoapertures (right column). Particle numbers, *N*, of less than one molecule in the excitation volume for both cases were confirmed using FCS, i.e., $G(\tau) > 1$ at $\tau = 0$. At first glance, the two-dimensional distributions of molecular species in the *E*−*S* histograms in Figure 5 appear to be similar for the experiments conducted in the diffraction-limited laser spot

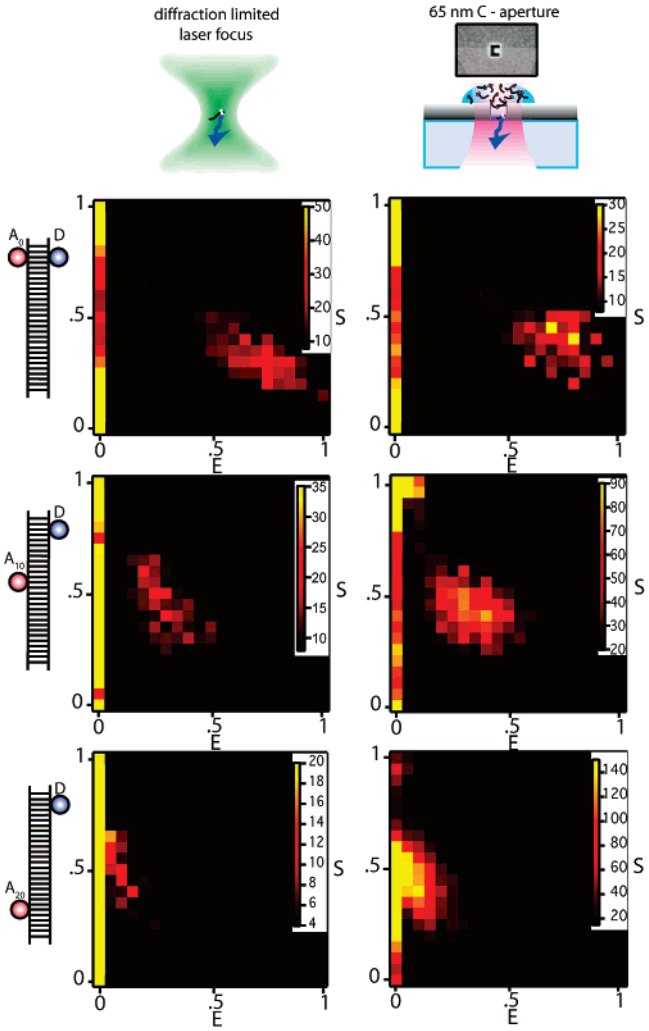

Figure 5. Two-dimensional *E*−*S* histograms for three DNA samples with different donor−acceptor distances as indicated by the cartoons to the left of the figure. The left-hand column corresponds to measurements conducted inside a diffraction-limited laser focus, and the right-hand column shows data from a C-aperture. Donor−acceptor distances increase from top to the bottom. These histograms show the full set of data without processing, i.e., donor-only and acceptor-only species have not been filtered out of these 2-D distributions.

and the aperture when comparing the results for the same donor−acceptor distance DNA duplex. In all *E*−*S* plots, three distinct molecule populations corresponding to donor-only (upper left corner, $E = 0$, $S = 1$), acceptor-only (lower left corner, $E = 0$, $S = 0$), and donor−acceptor pair samples (broader, remaining distributions roughly in the center of the plot) can be seen, with S centered approximately around 0.4. The shift from high FRET efficiency to low FRET efficiency for increasing donor−acceptor pair distance is observed in both cases with similar *E* values.

The 2-D histograms in Figure 5 can be filtered to eliminate donor-only and acceptor-only species. After free donor and free acceptor species have been removed, *E*−*S* histograms yield very similar distributions, shown in Figure 6, for measurements conducted in the diffraction-limited laser spot compared to the C-aperture. That is, *E* again shifts to lower values with increasing donor−acceptor distance, and *S* stays

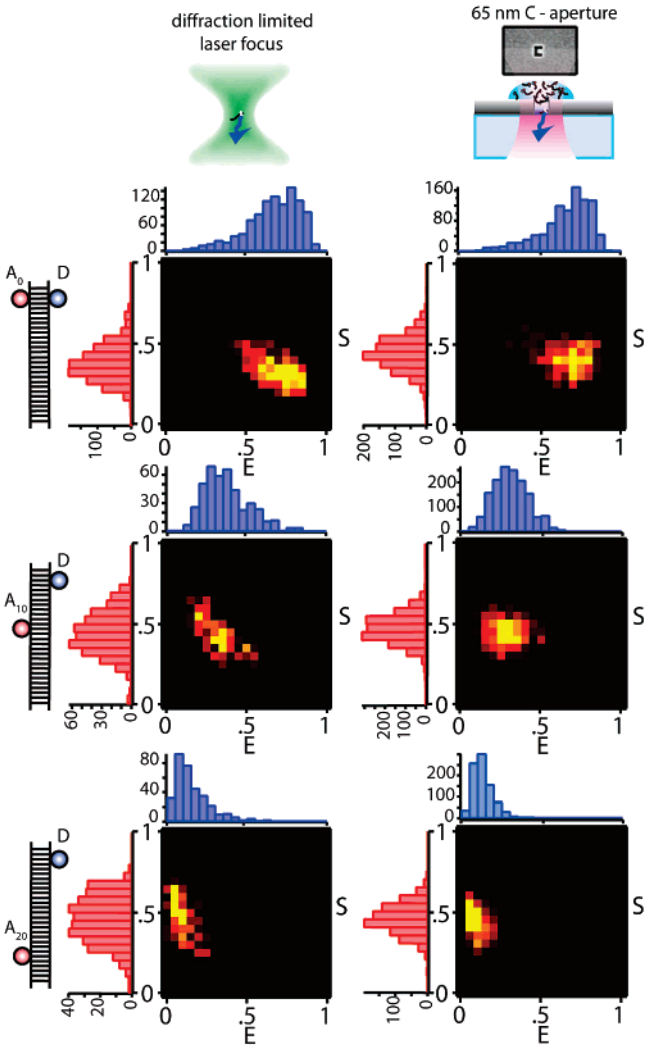

Figure 6. *E*−*S* histograms for the same DNA duplex samples as shown in Figure 5. Here, donor-only and acceptor-only species have been eliminated from the distributions based on time-gating criteria as described in Figure 2. The column on the left-hand side corresponds to measurements inside a diffraction-limited laser focus, and the right-hand column shows data from a C-aperture. Donor to acceptor distance increases from top to bottom.

the same in all cases, 0.4, corresponding to a 1:1 donor−acceptor ratio. Hence, this proves that PIE-FRET measurements can be successfully carried out at concentrations at least 1000 times higher than in diffraction-limited laser spots.

To illustrate that PIE-FRET inside nanoapertures can be used for quantitive analysis of the stoichiometry of donor−acceptor pairs, measurements were also conducted on DNA duplex samples with different donor−acceptor distances and donor−acceptor ratios. In particular, we studied 2 donor:1 acceptor and 1 donor:2 acceptor systems in which the individual donor and acceptor distances were always 10 base pairs. The DNA duplexes are illustrated in Figure 7, next to their resulting filtered *E*−*S* histograms. The measurements were again conducted in 65 nm C-apertures at 250 nM and at 50 pM in the diffraction-limited laser focus examples. Because of dye photobleaching, especially in the case of the acceptor dye, two populations with slightly different *E* and *S* values are observed. However, the same trends are

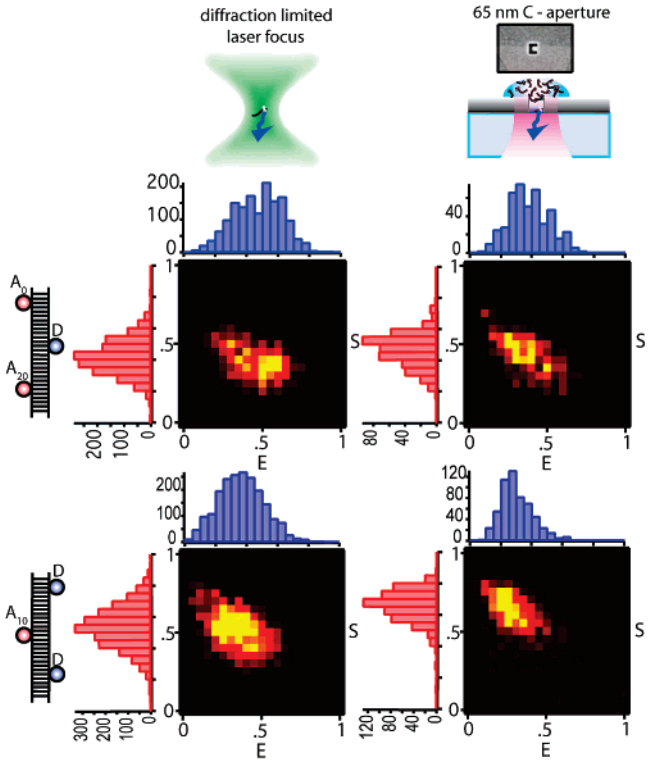

Figure 7. *E*−*S* histograms for DNA duplex samples with different donor−acceptor stoichiometry. The column on the left-hand side corresponds to measurements inside a diffraction-limited laser focus, and the right-hand column shows data from a C-aperture. Donor-only and acceptor-only species have been eliminated from the distributions based on arrival time-gating.

observed when comparing the results from the nanoaperture experiments to those from the diffraction-limited laser focus experiments. Different values of *E* for donor:acceptor stoichiometries other than 1:1 are expected and observed in our results. For example, a FRET complex with 2 donors and 1 acceptor will have a lower apparent FRET efficiency than that for a 1:1 donor−acceptor FRET complex with the same donor−acceptor distances, as the overall $F^{\mathrm{Dem}}_{\mathrm{Dex}}$ term in the expression will be larger due to the presence of two donors. For more details on FRET calculations with different numbers of donor and acceptors, see refs 30,31.

Conclusions. We have shown that the use of FIB-milled nanoapertures can extend quantitative molecular interaction experiments to a concentration range that is at least 3 orders of magnitude higher than what is possible with standard confocal microscopy techniques. This opens the door to the quantitative investigation of biological interactions that are otherwise not accessible, e.g., protein-binding interactions with nM to μM equilibrium binding constants. The C-aperture geometry is unique to our studies, and we have demonstrated that the use of these apertures for investigating biological interactions is equally valid when compared to apertures with different geometries, e.g., circular or square. The C-apertures may also have advantages over these other geometries, which will prove particularly true when extending these measurements to multiphoton excitation at near-infrared wavelengths.[29] For example, according to our preliminary results, the fields inside the C-aperture may be

enhanced 2−4 times for a given excitation wavelength and size aperture. Dye photobleaching is a potential drawback to calculating accurate $E-S$ distributions using PIE-FRET. However, there are many solutions available to decrease dye photobleaching such as the use of reducing agents in the buffer and a choice of different dyes less susceptible to photobleaching. Alternatively, various analysis tools have been developed to account for photobleaching in the data set.[32,33] These tools have not been implemented in this study, however, as the goal was to demonstrate the ability to perform PIE-FRET at biologically relevant concentrations inside FIB-milled nanoapertures. Thus, we conclude that this is the case, and even with short DNA duplex oligomers as test samples, there are advantages to conducting biological experiments at higher concentrations. We observed a surprising DNA denaturing effect at pM concentrations, even in the presence of high salt concentration and other reagents to stabilize DNA duplexes, which could be avoided at higher DNA concentrations inside C-apertures. This effect can limit single-molecule experiments utilizing short segments of DNA. Indeed, PIE-FRET provides a means for eliminating populations of donor-only and acceptor-only species. However, this requires each strand to be labeled with either a donor or acceptor molecule. Furthermore, investigations of protein−DNA binding interactions could potentially be disrupted by the presence of single-stranded DNA, again providing an incentive to make use of methods that reduce the effective volume.

Acknowledgment. We thank Dr. Ted Laurence for providing the Alexa dye modified DNA oligomers used in preparing the DA_{0-20} DNA duplex samples. Funding for this work was provided through the Center for Biophotonics, an NSF Science and Technology Center, managed by the University of California, Davis, under Cooperative Agreement no. PHY 0120999. T. Huser also acknowledges support by the Clinical Translational Science Center under grant no. UL1 RR024146 from the National Center for Research Resources (NCRR), a component of the National Institutes of Health (NIH), and NIH Roadmap for Medical Research.

Supporting Information Available: FDTD simulations; E and S calculation and 2-D $E-S$ histogram analysis. This material is available free of charge via the Internet at http://pubs.acs.org.

References

(1) Deniz, A. A.; Laurence, T. A.; Dahan, M.; Chemla, D. S.; Schultz, P. G.; Weiss, S. *Annu. Rev. Phys. Chem.* **2001**, *52*, 233−253.
(2) Jares-Erijman, E. A.; Jovin, T. M. *Nat. Biotechnol.* **2003**, *21*, 1387−1395.
(3) Sekar, R. B.; Periasamy, A. *J. Cell Biol.* **2003**, *160*, 629−633.
(4) Ha, T.; Enderle, T.; Ogletree, D. F.; Chemla, D. S.; Selvin, P. R.; Weiss, S. *Proc. Natl. Acad. Sci. U.S.A.* **1996**, *93*, 6264−6268.
(5) Deniz, A. A.; Laurence, T. A.; Beligere, G. S.; Dahan, M.; Martin, A. B.; Chemla, D. S.; Dawson, P. E.; Schultz, P. G.; Weiss, S. *Proc. Natl. Acad. Sci. U.S.A.* **2000**, *97*, 5179−5184.
(6) Laurence, T. A.; Kong, X. X.; Jager, M.; Weiss, S. *Proc. Natl. Acad. Sci. U.S.A.* **2005**, *102*, 17348−17353.
(7) Heilemann, M.; Tinnefeld, P.; Mosteiro, G. S.; Parajo, M. G.; Van, Hulst, N. F.; Sauer, M. *J. Am. Chem. Soc.* **2004**, *126*, 6514−6515.
(8) Tinnefeld, P.; Sauer, M. *Angew. Chem., Int. Ed.* **2005**, *44*, 2642−2671.
(9) Kim, H. D.; Nienhaus, G. U.; Ha, T.; Orr, J. W.; Williamson, J. R.; Chu, S. *Proc. Natl. Acad. Sci. U.S.A.* **2002**, *99*, 4284−4289.
(10) Blanchard, S. C.; Gonzalez, R. L.; Kim, H. D.; Chu, S.; Puglisi, J. D. *Nat. Struct. Mol. Biol.* **2004**, *11*, 1008−1014.
(11) Rueda, D.; Bokinsky, G.; Rhodes, M. M.; Rust, M. J.; Zhuang, X. W.; Walter, N. G. *Proc. Natl. Acad. Sci. U.S.A.* **2004**, *101*, 10066−10071.
(12) Kapanidis, A. N.; Lee, N. K.; Laurence, T. A.; Doose, S.; Margeat, E.; Weiss, S. *Proc. Natl. Acad. Sci. U.S.A.* **2004**, *101*, 8936−8941.
(13) Kapanidis, A. N.; Laurence, T. A.; Lee, N. K.; Margeat, E.; Kong, X. X.; Weiss, S. *Acc. Chem. Res.* **2005**, *38*, 523−533.
(14) Muller, B. K.; Zaychikov, E.; Brauchle, C.; Lamb, D. C. *Biophys. J.* **2005**, *89*, 3508−3522.
(15) Ruttinger, S.; MacDonald, R.; Kramer, B.; Koberling, F.; Roos, M.; Hildt, E. *J. Biomed. Opt.* **2006**, *11*, 024012.
(16) Lee, N. K.; Kapanidis, A. N.; Wang, Y.; Michalet, X.; Mukhopadhyay, J.; Ebright, R. H.; Weiss, S. *Biophys. J.* **2005**, *88*, 2939−2953.
(17) Kapanidis, A. N.; Margeat, E.; Ho, S. O.; Kortkhonjia, E.; Weiss, S.; Ebright, R. H. *Science* **2006**, *314*, 1144−1147.
(18) Kapanidis, A. N.; Margeat, E.; Laurence, T. A.; Doose, S.; Ho, S. O.; Mukhopadhyay, J.; Kortkhonjia, E.; Mekler, V.; Ebright, R. H.; Weiss, S. *Mol. Cell* **2005**, *20*, 347−356.
(19) Muller, B. K.; Reuter, A.; Simmel, F. C.; Lamb, D. C. *Nano Lett.* **2006**, *6*, 2814−2820.
(20) Laurence, T. A.; Youngeun, K.; Yin, E.; Hollars, C. W.; Camarero, J. A.; Barsky, D. *Biophys. J.* **2007**, *92*, 2184−2198.
(21) Lee, N. K.; Kapanidis, A. N.; Koh, H. R.; Korlann, Y.; Ho, S. O.; Kim, Y.; Gassman, N.; Kim, S. K.; Weiss, S. *Biophys. J.* **2007**, *92*, 303−312.
(22) Ross, J.; Buschkamp, P.; Fetting, D.; Donnermeyer, A.; Roth, C. M.; Tinnefeld, P. *J. Phys. Chem. B* **2007**, *111*, 321−326.
(23) Levene, M. J.; Korlach, J.; Turner, S. W.; Foquet, M.; Craighead, H. G.; Webb, W. W. *Science* **2003**, *299*, 682−686.
(24) Samiee, K. T.; Moran-Mirabal, J. M.; Cheung, Y. K.; Craighead, H. G. *Biophys. J.* **2006**, *90*, 3288−3299.
(25) Wenger, J.; Conchonaud, F.; Dintinger, J.; Wawrezinieck, L.; Ebbesen, T. W.; Rigneault, H.; Marguet, D.; Lenne, P. F. *Biophys. J.* **2007**, *92*, 913−919.
(26) Mannion, J. T.; Craighead, H. G. *Biopolymers* **2007**, *85*, 131−143.
(27) Genet, C.; Ebbesen, T. W. *Nature* **2007**, *445*, 39−46.
(28) Matteo, J. A.; Fromm, D. P.; Yuen, Y.; Schuck, P. J.; Moerner, W. E.; Hesselink, L. *Appl. Phys. Lett.* **2004**, *85*, 648−650.
(29) Tang, L.; Miller, D. A. B.; Okyay, A. K.; Matteo, J. A.; Yuen, Y.; Saraswat, K. C.; Hesselink, L. *Opt. Lett.* **2006**, *31*, 1519−1521.
(30) Corry, B.; Jayatilaka, D.; Rigby, P. *Biophys. J.* **2005**, *89*, 3822−3836.
(31) Pons, T.; Medintz, I. L.; Wang, X.; English, D. S.; Mattoussi, H. *J. Am. Chem. Soc.* **2006**, *128*, 15324−15331.
(32) Eggeling, C.; Widengren, J.; Brand, L.; Schaffer, J.; Felekyan, S.; Seidel, C. A. M. *J. Phys. Chem. A* **2006**, *110*, 2979−2995.
(33) Nir, E.; Michalet, X.; Hamadani, K. M.; Laurence, T. A.; Neuhauser, D.; Kovchegov, Y.; Weiss, S. *J. Phys. Chem. B* **2006**, *110*, 22103−22124.

NL070822V